Journal of Engineering Mathematics **45:** 75–90, 2003.
© 2003 *Kluwer Academic Publishers. Printed in the Netherlands.*

A mathematical model for wet-chemical diffusion-controlled mask etching through a circular hole

H.K. KUIKEN
Twente University of Technology, Faculty of Applied Mathematics, P.O. Box 217, 7500 AE Enschede, The Netherlands

Received 17 July 2002, accepted in revised form 1 October 2002

Abstract. Asymptotic solutions are presented for diffusion-controlled wet-chemical etching through a round hole in a mask. The three-dimensional diffusion field is assumed to be axisymmetric and fully developed. Two time regimes are considered. The first applies when the etched depth is small in comparison with the width of the mask opening. In the second, the depth of etching is much greater than the width of the mask opening. Explicit solutions are found for the shape of the etched surface as a function of the physical parameters. Among other things it is found that, as long as the etched pits are shallow, etching through small apertures is faster than through larger ones. The opposite is true for deep pits.

Key words: asymptotics, diffusion-controlled, etching, mask, oblate spheroidal coordinates

This paper is dedicated to Hendrik W. Hoogstraten who served the Journal of Engineering Mathematics as Managing Editor from 1975 until 1990.

1. Introduction

Diffusion-controlled isotropic etching is a technique by which a solid, immersed in an acid solution, is dissolved by a fast chemical process that occurs at the surface of the solid. The solid is either amorphous, *e.g.* glass, or when it has a crystal structure, as is the case for silicon, the etch rate is independent of the crystallographic orientation. During the chemical reaction the material of the solid and agents in the acid interact in such a way that the solid material dissolves. This process is used in many technological applications, such as polishing and the production of objects of a desired shape. In the latter of these applications, the surface of the body is partly covered with an impenetrable layer, the mask, which prevents the underlying solid from being attacked directly by the acid. Thus, only selected parts of the body will be etched. For obvious reasons, this technique is called mask etching. For further information on wet-chemical etching we refer to [1,2,3].

Although etching has been known for a very long time, the mathematical modelling of diffusion-controlled etching, for non-trivial geometries, is fairly recent. The so-called edge effect, which implies large etch rates near mask edges, was described conclusively only as late as 1984 [4]. Experimental verification of the theory developed in [4] was furnished by two subsequent papers [5,6]. Two-dimensional etching through a slit was described in [7,8]. The first of these publications gives asymptotic analytic solutions valid for various time regimes. In reference [8] a numerical technique was applied to solve the basic equations. The results of [7] and [8] agree well for the time regimes considered.

Recently, further research has been done on diffusion-controlled isotropic etching, with the attention being focussed on experimental techniques [9]. Interesting results were obtained for

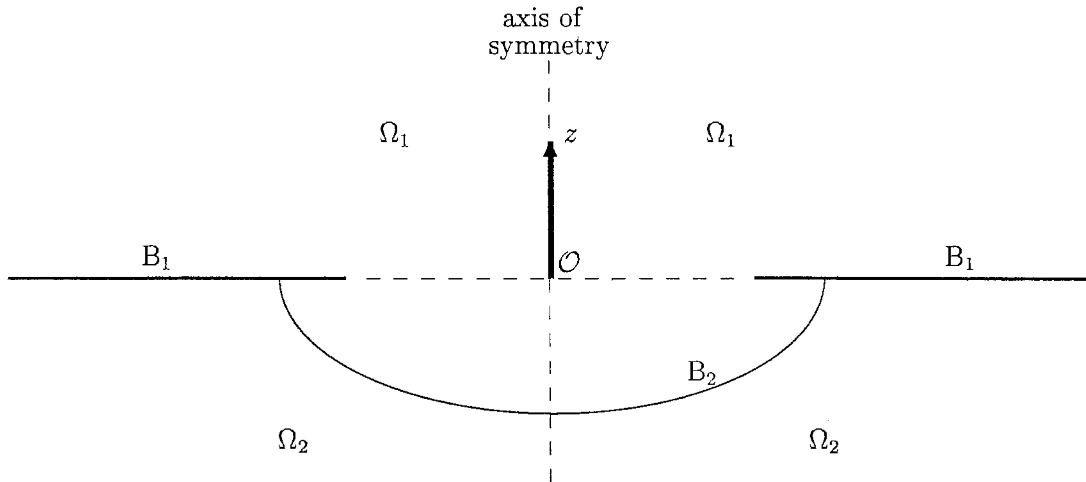

Figure 1. Geometrical sketch

the etching of wide slits, showing the mask-edge effect; another range of results were given for deep etching through narrow slits. In the latter, depths of more than ten times the widths of the mask openings were attained. The latter results clearly belong to the late-time regime for which an analytic solution of an asymptotic nature was developed in [7], describing etching through a slit.

A problem that is still open for mathematical modelling is etching through a round aperture in a mask. In this paper we shall tackle this problem by applying asymptotic methods of a kind considered in [7] to derive approximate solutions for various time regimes. Experimental verification of our findings is still lacking. The solutions, however, are sufficiently interesting in their own right, in that they provide a clear insight into the parameter dependence of the salient etching characteristics, both in the early- and late-time regimes. It is hoped that these results will prompt careful experiments to confirm (or disprove?) these findings.

2. Mathematical model

2.1. Description of the problem

Let us consider a rotationally symmetric geometry as depicted in Figure 1. An etching liquid or etchant occupies the region Ω_1, which is assumed to extend infinitely far upwards. The region Ω_2 extends infinitely far downwards and is filled with the material that is to be etched. The boundary separating the regions Ω_1 and Ω_2 consists of two rotationally symmetric parts, namely B_1, which is a permanently impermeable sheet that prevents the etchant from attacking the solid, and B_2, which is the etching surface. The latter is a moving boundary; initially it is the flat circular part $P\backslash B_1$, where P is the entire plane in which B_1 lies. B_1 is called the mask.

If the concentration of the active etching component in the etchant is denoted by c (kmol/m^3), then, in the absence of fluid motion, the diffusion equation holds:

$$\frac{\partial c}{\partial t} = D\nabla^2 c \quad \text{in} \quad \Omega_1 , \quad (t \geq 0) . \tag{1}$$

Here t is the time and D (m^2/s) is the diffusion coefficient.

Assuming a diffusion-controlled process, which means that the reaction at the etching surface B_2 proceeds 'infinitely' fast, we have the boundary condition

$$c = 0 \quad \text{on} \quad B_2 . \tag{2}$$

In physical terms this condition can be explained as follows: if an active ion, represented by c, is reacted away infinitely fast during the etch reaction, it will be impossible for diffusion to replace it by another within a finite time. A diffusion gradient normal to the wall will be set up, down which the ions diffuse towards the surface. It is impossible for a positive value of c to be maintained at B_2 and, consequently, the concentration will assume the lowest possible value there, which is zero.

Since the boundary B_2 is moving, which means that its position is an unknown of the problem, a second boundary condition is needed. This condition follows from the relation between the rate of dissolution of the etching boundary B_2 and the gradient of c. This is usually given as

$$\boldsymbol{v} = -\sigma_e \nabla c \quad \text{on} \quad B_2 , \tag{3}$$

where $\boldsymbol{v}$ is the normal velocity at which the surface B_2 proceeds into the solid Ω_2. Further, ∇c is the concentration gradient at B_2 and σ_e is the etching parameter. It can be shown that (3) may be put in the more restricted form

$$v_n = -\sigma_e \boldsymbol{n} \cdot \nabla c , \tag{4}$$

where v_n is the normal speed at which the surface B_2 moves in the direction of Ω_2 and $\boldsymbol{n}$ is the normal to B_2 pointing into Ω_2.

The condition on the permanent boundary B_1 reads

$$\boldsymbol{n} \cdot \nabla c = 0 , \tag{5}$$

expressing the inertness of the mask. At infinity we have

$$c \to c_0 \quad \text{for} \quad r \to \infty , \tag{6}$$

where r is a radius vector with origin at $\mathcal{O}$. Here c_0 is the concentration of the active etching component in pure etchant.

The problem is completed by the initial conditions

$$B_2 = P \backslash B_1 , \tag{7}$$

$$c \equiv c_0 \quad \text{everywhere in} \quad \Omega_1 \tag{8}$$

at $t = 0$.

2.2. Oblate spheroidal coordinates

Let us begin by defining a Cartesian coordinate system x, y, z, where z measures distance from the plane of the mask B_1 as seen from Ω_1. The coordinates x and y are in this plane with origin at $\mathcal{O}$. On the basis of this coordinate system we now define oblate spheroidal coordinates η, θ, φ as follows:

$$x = a \cosh \eta \ \cos \theta \ \cos \varphi , \tag{9}$$

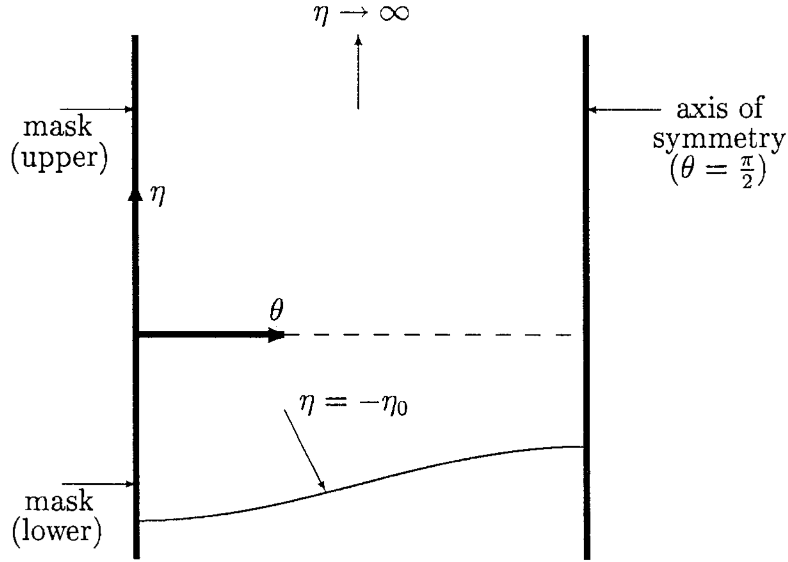

Figure 2. Geometry in oblate spheroidal coordinates

$$y = a \cosh \eta \ \cos \theta \ \sin \varphi \,, \tag{10}$$

$$z = a \sinh \eta \ \sin \theta \,, \tag{11}$$

where a is the radius of the orifice $P \backslash B_1$. The ranges of the various variables are

$$-\eta_0(\theta, t) < \eta < \infty \quad 0 \le \theta \le \tfrac{1}{2}\pi \,, \quad 0 \le \varphi \le 2\pi \,, \tag{12}$$

where $-\eta_0(\theta, t)$ coincides with the etching surface B_2; $\eta_0 \equiv 0$ at $t = 0$ and is a positive function of θ and t afterwards. Because of the rotational symmetry, that is, symmetry with respect to the z-axis, the concentration c is independent of φ. The mask B_1 is represented by $\theta = 0$ and the z-axis by $\theta = \frac{1}{2}\pi$; this applies to both the upper and lower parts of B_1. Regions in Ω_1 that are infinitely far from the origin $\mathcal{O}$ are represented by $\eta \to \infty$; see Figure 2 for the transformed geometry. Oblate spheriodal coordinates are described in [10, pp. 31–34], but the ranges of the coordinates η and θ used there differ from ours.

In terms of these new coordinates, the governing equation (1) reads

$$a^2(\cosh^2 \eta - \cos^2 \theta)\frac{\partial c}{\partial t} = D \left(\frac{\partial^2 c}{\partial \eta^2} + \tanh \eta \frac{\partial c}{\partial \eta} + \frac{\partial^2 c}{\partial \eta^2} - \tan \theta \frac{\partial^2 c}{\partial \theta^2} \right) \,. \tag{13}$$

The transformed boundary conditions are:

$$c = 0 \quad \text{at} \quad \eta = -\eta_0 \,, \tag{14}$$

$$\frac{\partial c}{\partial \theta} = 0 \quad \text{at} \quad \theta = 0 \,, \tag{15}$$

$$\frac{\partial c}{\partial \theta} = 0 \quad \text{at} \quad \theta = \tfrac{1}{2}\pi \,, \tag{16}$$

$$c \to c_0 \quad \text{for} \quad \eta \to \infty \,. \tag{17}$$

Initially ($t = 0$) we have

$$c \equiv 0 \quad \text{for} \quad 0 \le \eta \le \infty\,, \quad 0 \le \theta \le \tfrac{1}{2}\pi\,, \tag{18}$$

$$\eta_0(\theta, t) \equiv 0 \quad \text{for} \quad 0 \le \theta \le \tfrac{1}{2}\pi\,. \tag{19}$$

To complete the model, we need to consider the moving-boundary condition (3). It was argued earlier [4] that this condition can be expressed as

$$\frac{\partial f}{\partial t} + \boldsymbol{v} \cdot \nabla f = 0\,, \tag{20}$$

where f is a functional description of the moving boundary, *e.g.*, $f(x, y, z, t) = 0$ and ∇ is the spatial gradient operator. Substitution of (3) in (20) gives

$$\frac{\partial f}{\partial t} = \sigma_{\mathrm{e}} \nabla c \cdot \nabla f\,. \tag{21}$$

In terms of oblate spheroidal coordinates this reads:

$$a^2(\cosh^2 \eta - \cos^2 \theta)\frac{\partial f}{\partial t} = \sigma_{\mathrm{e}} \left(\frac{\partial c}{\partial \eta}\frac{\partial f}{\partial \eta} + \frac{\partial c}{\partial \theta}\frac{\partial f}{\partial \theta} \right)\,, \tag{22}$$

where again rotational symmetry has been assumed.

We can now be more specific about f. Let us represent it by $\eta + \eta_0(\theta, t)$, *i.e.*, let the moving surface be given by $\eta = -\eta_0(\theta, t)$. Equation (22) can then be written as

$$a^2(\cosh^2 \eta_0 - \cos^2 \theta)\frac{\partial \eta_0}{\partial t} = \sigma_{\mathrm{e}} \left(\frac{\partial c}{\partial \eta} + \frac{\partial c}{\partial \theta}\frac{\partial \eta_0}{\partial \theta} \right)\bigg|_{\eta = -\eta_0}\,. \tag{23}$$

2.3. Dimensionless representation

In order to be able to make sensible judgments about the various physical regimes to which this problem applies, it is of paramount importance that the model be represented in dimensionless form. Let us introduce the following dimensionless concentration and time, C and τ, as follows:

$$C = 1 - \frac{c}{c_0}\,, \quad \tau = \frac{D}{a^2}t\,. \tag{24}$$

The governing equation now reads:

$$\frac{\partial C}{\partial \tau} = \frac{1}{\cosh^2 \eta - \cos^2 \theta} \left(\frac{\partial^2 C}{\partial \eta^2} + \tanh \eta \frac{\partial C}{\partial \eta} + \frac{\partial^2 C}{\partial \theta^2} - \tan \theta \frac{\partial C}{\partial \theta} \right) \tag{25}$$

and the moving-boundary condition is

$$\frac{\partial \eta_0}{\partial \tau} = -\frac{1}{\beta}\frac{1}{\cosh^2 \eta_0 - \cos^2 \theta} \left(\frac{\partial C}{\partial \eta} + \frac{\partial C}{\partial \theta}\frac{\partial \eta_0}{\partial \theta} \right)\bigg|_{\eta = -\eta_0}\,. \tag{26}$$

The other boundary condition on the moving boundary is

$$C = 1 \quad \text{at} \quad \eta = -\eta_0(\theta, \tau) \tag{27}$$

and that at infinity reads:

$$C \to 0 \quad \text{for} \quad \eta \to \infty \,. \tag{28}$$

The model is completed by conditions similar to those of Equations (15), (16), (18) and (19), where it is understood that Equation (18) applies for $C = 1$.

The dimensionless model adequately describes diffusion-controlled etching through a circular orifice and contains only a single dimensionless parameter, β, which is defined as follows in terms of the dimensional physical parameters:

$$\beta = \frac{D}{\sigma_e c_0} \,. \tag{29}$$

The very nature of β suggests that it measures the relative importance of diffusional and surface effects. A more precise analysis of β was given in [5], where it was argued that it is a ratio of volumes, namely of that of the molecules in solution, divided by that occupied by these same molecules in the solid. Estimates of β can be found in [5] for a range of etching systems that are known to be diffusion-controlled. The lowest value reported in [5] is $\beta = 100$. Most of the other systems considered in that paper, with very common and frequently used systems among them, show much larger values of β, even as large as 10,000. Thus, we may assume that it is in the nature of β to be large, so that asymptotic methods can be brought to bear to simplify problems of the kind considered here.

3. Solutions for small cavities

Looking at the dimensionless time τ, as given by Equation (24), we can draw an important conclusion for the etching of small cavities. Typical values of the diffusion coefficient D are in the range of 10^{-9}–10^{-10} m^2/s. This means that, for holes smaller than ten microns (10^{-5} m), the dimensionless time τ is larger than unity when the actual time of etching, t, exceeds one second. Since a typical etching process lasts several minutes, it follows that, for these small cavities, most of the etching process evolves in the large-time regime. In modern micromechanical technology, cavities as small as ten microns, or even smaller, are quite common. Thus, there is ample reason to study the large-time regime for etching through a circular mask opening.

Another reason to pay special attention to small cavities in the context of this paper is that the exclusion of convection effects is realistic only in the case of small cavities. It is the Péclet number

$$\text{Pe} = \frac{Ua}{D} \tag{30}$$

which decides whether or not convection must be taken into account. Here U is a typical velocity in the vicinity of the etching cavity. Supposing the velocity gradient of the flow outside the cavity is α, we may estimate U by

$$U \sim \alpha a \,. \tag{31}$$

This shows that the value of the Péclet number decreases in proportion to the square of the size of the cavity. Since D is very small, as was shown above, a must be reduced considerably for Pe to become much less than unity, which is the condition that decides if convection effects can be excluded.

For a source of constant strength and shape a three-dimensional diffusion field becomes stationary for sufficiently long times. By source we mean that a value of the field variable, here C, is imposed at a fixed location for the duration of the process. In etching C is held at the value 1 on the bounded etching surface, so the strength is indeed constant. However, the shape of the source is not, but slowly varying, or rather slowly progressing. Thus, the 'stationary' diffusion field is dragged along with the slowly progressing source. The latter becomes important when the etching surface has progressed deeply into the material, that is, far below the mask.

3.1. Shallow cavities

3.1.1. *Outer solution*

Since the dimensionless etching parameter β, as defined by Equation (29), is very large, the etching surface has hardly moved when the diffusion field has already reached a quasi-stationary state. It is useful, therefore, to consider the problem defined by the time-indepedent version of Equation (25), namely

$$\frac{\partial^2 C}{\partial \eta^2} + \tanh \eta \frac{\partial C}{\partial \eta} + \frac{\partial^2 C}{\partial \theta^2} - \tan \theta \frac{\partial C}{\partial \theta} = 0 \tag{32}$$

in

$$0 \leq \eta < \infty\,, \quad 0 \leq \theta \leq \tfrac{1}{2}\pi\,, \tag{33}$$

where the use of the boundary $\eta = 0$ points to the fact that the etching boundary has not moved significantly and can be approximated by this value, which is a zeroth-order approximation.

Since the boundary conditions are those defined by (14–17) with $\eta_0 \equiv 0$, the solution is simply

$$C = 2 - \frac{4}{\pi} \arctan \mathrm{e}^{\eta}\,, \tag{34}$$

whence, to leading order,

$$\frac{\partial C}{\partial \eta} = -\frac{2}{\pi} \frac{1}{\cosh \eta}\,, \quad \frac{\partial C}{\partial \theta} = 0\,. \tag{35}$$

This can be substituted in (26) to yield a leading-order equation for the displacement of the etching boundary:

$$(\cosh^2 \eta_0 - \cos^2 \theta) \cosh \eta_0 \frac{\partial \eta_0}{\partial \tau} = \frac{2}{\pi} \frac{1}{\beta}\,; \quad \eta_0 \equiv 0 \quad \text{at} \quad \tau = 0\,. \tag{36}$$

This yields

$$\tfrac{1}{3} \sinh^3 \eta_0 + \sin^2 \theta \sinh \eta_0 = \frac{2}{\pi} \frac{1}{\beta} \tau\,. \tag{37}$$

The interpretation of this equation requires some care. We should realize that the analysis of this section applies for small values of η_0, *i.e.*, $0 \leq \eta_0 \ll 1$. Thus, the right-hand side of (37) must be small, so that

$$1 \ll \tau \ll \beta\,. \tag{38}$$

This is a realistic condition, since $\beta \gg 1$. The left-hand part of (38) expresses the large-time condition for an almost stationary diffusion field.

Since $\eta_0 \ll 1$, the second term on the left-hand side of Equation (37) dominates, except when θ is sufficiently close to zero. Thus, away from the mask edge, the solution for η_0 is approximately given by

$$\eta_0 \sim \frac{2}{\pi}\frac{1}{\beta}\frac{\tau}{\sin^2\theta} \tag{39}$$

or in dimensional Cartesian coordinates:

$$\frac{z}{a} \sim \frac{2}{\pi}\frac{\tau}{\beta}\frac{a}{\sqrt{a^2 - x^2 - y^2}}\,. \tag{40}$$

This expression clearly fails near the mask edge, that is for $\theta = 0$ or $x^2 + y^2 = a^2$, Equation (37) shows that the left-most term on the left dominates when $\theta \downarrow 0$ and the solution at $\theta = 0$ would appear to be given by

$$\eta_0 \sim \left(\frac{6}{\pi}\frac{\tau}{\beta}\right)^{\frac{1}{3}}\,. \tag{41}$$

However, this solution is false! The analysis of a related problem studied in [4] shows that the displacement of the boundary is a leading-order phenomenon in the immediate vicinity of the mask edge. It cannot be obtained by a straightforward perturbation approach of a kind as used above. The correct approach is similar to that followed in [4] and is presented in the following subsection; see Equation (64).

3.1.2. *Mask-edge region. Inner solution*

For a proper description of the problem in the mask-edge region we introduce scaled variables $\bar{\theta}$, $\bar{\eta}$, $\bar{\eta}_0$ and $\bar{C}$ as follows:

$$(\theta, \eta, \eta_0) = \beta^{-1/3}(\bar{\theta}, \bar{\eta}, \bar{\eta}_0), \qquad C = 1 - \beta^{-1/3}\bar{C}\,. \tag{42}$$

Thus, for $\beta \gg 1$, the original variables θ, η, η_0 are $\ll 1$ and $C \sim 1$ for values of the new variables that are of order unity.

Substituting (42) in (32) and letting $\beta \to \infty$, we see that the governing field equation is reduced to

$$\frac{\partial^2\bar{C}}{\partial\bar{\theta}^2} + \frac{\partial^2\bar{C}}{\partial\bar{\eta}^2} = 0\,. \tag{43}$$

By the same token, and using

$$\cosh^2\bar{\eta}_0 - \cos^2\bar{\theta} = \beta^{-2/3}(\bar{\theta}^2 + \bar{\eta}_0^2) + \mathcal{O}(\beta^{-4/3})\,, \tag{44}$$

we can write the moving-boundary condition (26) as

$$\bar{\eta} + \bar{\eta}_0 = 0: \qquad \frac{\partial\bar{\eta}_0}{\partial\tau} = \frac{1}{\bar{\theta}^2 + \bar{\eta}_0^2}\left(\frac{\partial\bar{C}}{\partial\bar{\eta}} + \frac{\partial\bar{C}}{\partial\bar{\theta}}\frac{\partial\bar{\eta}_0}{\partial\bar{\theta}}\right)\,. \tag{45}$$

which shows indeed that the boundary displacement is now a leading-order effect, rather than a perturbation, as was the case with the problem of Section 3.1.1.

The other boundary condition on the moving boundary reads:

$$\bar{\eta} + \bar{\eta}_0 = 0: \qquad \bar{C} = 0. \tag{46}$$

It is understood that $\bar{\eta}_0$ is a function of both $\bar{\theta}$ and τ.

What remains is to define a condition for $\bar{\eta} \to \infty$. This is obtained by matching and a proper taking of limits. If in (42) a large, but fixed value of $\bar{\eta}$ is taken, upon which β is allowed to tend to infinity, then η is seen to approach zero. The mask-edge, or inner solution that we consider here is to merge smoothly with the outer solution (34) in the limit we defined a moment ago. Thus, all we have to do is to insert the transformed variables (42) into (34) and then expand for $\beta \to \infty$. This gives

$$1 - \beta^{-\frac{1}{3}}\bar{C} = 2 - \frac{4}{\pi}\arctan \mathrm{e}^{\beta^{-1/3}\bar{\eta}} = 1 - \frac{2}{\pi}\beta^{-1/3}\bar{\eta} + \mathcal{O}(\beta^{-2/3}). \tag{47}$$

From this we see that the following condition holds:

$$\bar{C} \to \frac{2}{\pi}\bar{\eta} \quad \text{for} \quad \bar{\eta} \to \infty. \tag{48}$$

Strictly speaking, we must also define a condition for $\bar{\theta} \to \infty$. Since, to first order, the outer solution does not depend on $\bar{\theta}$, we simply have, by a process similar to that which led to (48):

$$\frac{\partial \bar{C}}{\partial \bar{\theta}} \to \infty \quad \text{as} \quad \bar{\theta} \to \infty. \tag{49}$$

The problem defined by Equation (43) and the boundary conditions (15), (45), (46), (48) and (49) admits a similarity solution. To find it, let us introduce

$$(\bar{\theta}, \bar{\eta}, \bar{\eta}_0(\bar{\theta}, \tau)) = A\tau^{1/3}(\rho, \phi, \phi_0(\rho)), \quad \bar{C} = B\tau^{1/3}u, \tag{50}$$

where A and B are constants yet to be determined. Substitution in the above equations yields

$$\frac{\partial^2 u}{\partial \phi^2} + \frac{\partial^2 u}{\partial \rho^2} = 0, \tag{51}$$

$$\phi + \phi_0(\rho) = 0: \quad u = 0, \tag{52}$$

$$\frac{1}{3}A^4\left(\phi_0 - \rho\frac{\mathrm{d}\phi_0}{\mathrm{d}\rho}\right)(\phi_0^2 + \rho^2) = B\left(\frac{\partial u}{\partial \phi} + \frac{\partial u}{\partial \rho}\frac{\mathrm{d}\varphi_0}{\mathrm{d}\rho}\right), \tag{53}$$

$$\rho = 0: \quad \frac{\partial u}{\partial \rho} = 0, \tag{54}$$

$$\rho \to \infty: \quad \frac{\partial u}{\partial \rho} \to \infty, \tag{55}$$

$$\phi \to \infty: \quad u \to \frac{2}{\pi}\frac{A}{B}\phi. \tag{56}$$

By choosing

$$A = \left(\frac{3}{2\pi\sigma}\right)^{1/3}, \quad B = \frac{2}{\pi\sigma}\left(\frac{3}{2\pi\sigma}\right)^{1/3}, \tag{57}$$

where [4, Equation 49]

$$\sigma = \pi^{-3/2}\Gamma(\tfrac{1}{4}), \tag{58}$$

we see that the problem defined by (51)–(56) is exactly the same as that defined in [4, Equations (81–85)], where, for completeness, we have added condition (55) here. Thus, we can use the results obtained in [4].

3.1.3. *Zero-order approximation to full solution*

An approximate solution for η_0 that is uniformly valid for $\beta \gg 1$ and for all values of θ in the interval $0 \le \theta \le \frac{1}{2}\pi$, with the mask edge $\theta = 0$ included, can now be derived by a process similar to that explained in [4]. The leading term of a composite expansion is defined by

$$\eta_0|_{\text{inner}} + \eta_0|_{\text{outer}} - \text{common part}, \tag{59}$$

where the common part is the part that the inner and the outer expansions have in common at the level considered, which here is the zeroth order. In the previous two subsections we derived the leading terms of the expansions. Therefore, $\eta_0|_{\text{inner}}$ is approximated by the leading-order solution (39) and, from (42) and (50), the leading-order outer solution is $A(\tau/\beta)^{1/3}\phi_0$, where ϕ_0 is given by the values listed in [4, Table 2]. Later, Howison and King [11] succeeded in finding an analytic solution for ϕ_0. They used a method devised by Polubarinova-Kochina [12] to solve free-boundary problems in porous media.

We may obtain a leading-order expression for the common part by expressing (39) in terms of the inner variable (50), assuming a fixed, but large value of ρ and then looking at the behaviour for $\beta \to \infty$. This gives

$$\phi_0 \sim \frac{2}{\pi}\frac{1}{A^3\rho^2} = \frac{4}{3}\sigma\frac{1}{\rho^2}. \tag{60}$$

This corresponds with the result reported in [4, Table 2].

In view of the above, a leading-order expansion in β can now be given for the boundary displacement, namely

$$\eta_0 \sim \frac{2}{\pi}\frac{\tau}{\beta}\frac{1}{\sin^2\theta} + \left(\frac{\tau}{\beta}\right)^{1/3} A\left\{\phi_0(\rho) - \frac{4}{3}\sigma\frac{1}{\rho^2}\right\}. \tag{61}$$

Here we have used (39), (42), (50), (59) and (60).

This approximate solution is shown in Figure 3 for $0 \le \theta \le \frac{\pi}{2}$. Clearly, η_0 depends only on θ and the combination β/τ. By (38) the latter can only be assigned large values. When $\beta/\tau \downarrow 1$, the similarity part of the solution – this represents the solution in the mask-edge region – tends to fill the entire domain $0 \le \theta \le \frac{\pi}{2}$ and the solution has long since lost its validity. From then on another time regime sets in.

Using the coordinate transformation (9)–(11), we may recast (61) in terms of the more familiar Cartesian coordinates. Because of rotational symmetry, it is sufficient to present the function $z_0(r)$, where $r = \sqrt{x^2 + y^2}$, which is to be distinguished from the variable r used in Equation (6). From (9)–(11) and $\eta = -\eta_0(\theta, \tau)$, this function, representing the boundary displacement, is given implicitly by

$$r = a\cosh\eta_0\cos\theta\,; \quad z_0 = -a\sinh\eta_0\sin\theta \tag{62}$$

together with Equation (61). This function is depicted in Figure 4 for various values of the reduced time τ/β. Clearly, the edge effect is relatively strongest for small values of the time.

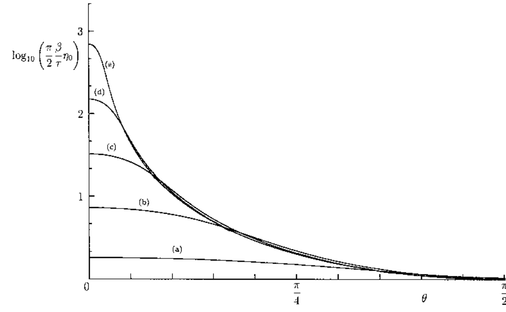

Figure 3. Leading-order composite expansion for boundary displacement $\eta_0(\theta)$ defined by Equation (61) for: (a) $\beta/\tau = 1$, (b) $\beta/\tau = 10$, (c) $\beta/\tau = 100$, (d) $\beta/\tau = 1000$, and (e) $\beta/\tau = 10000$.

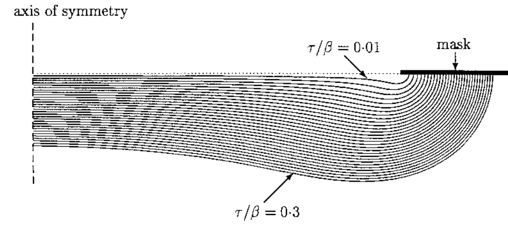

Figure 4. Evolution of the etching boundary $-z_0(r)$ as a function of τ/β. Curves depicted are for $\tau/\beta =$ 0·01 (0·01) 0·3. Here z_0 measures distance from the plane of the mask and r distance from the axis of symmetry.

This is also borne out by the fact that, in the immediate vicinity of the mask, the etched depth is proportional to $(\tau/\beta)^{1/3}$ (see Equation (63) below), whereas in the central part of the aperture etching proceeds in proportion to τ/β (see Equation (39)).

To conclude this section, we return to the spurious value $\eta_0|_{\theta=0}$ given by Equation (41). The correct asymptotic approximation follows from (61) by letting $\theta \downarrow 0$. The singular behaviour of the first term on the right is cancelled by an equally singular term to the far right, whence we have

$$\eta_0|_{\theta=0} = A\left(\frac{\tau}{\beta}\right)^{1/3} \phi_0(0) + \mathcal{O}(\tau/\beta)\,. \tag{63}$$

Since $\phi_0(0) \approx 1{\cdot}042$ (from [4]), or $\phi_0(0) = \sigma^{1/3}3^{1/6}$ (from [11][1], we have

$$\eta_0|_{\theta=0} = 3^{1/2}(2\pi)^{-1/3}\left(\frac{\tau}{\beta}\right)^{1/3} \approx 0{\cdot}939\left(\frac{\tau}{\beta}\right)^{1/3}\,. \tag{64}$$

The corresponding coefficient in (41) is 1·241. Thus, the spurious solution (41) overestimates the strength of the edge effect. This can be explained by the following argument. Equation (41) was obtained by the analysis of a model that assumed a flat immovable surface from which diffusion could take place freely in all directions above it in a three-dimensional space. The correct analysis, however, involves, to first order, an etching surface that is partly overhung by a mask. Diffusional transport in all directions in the space above the mask is possible only after transport of the etched materials has been encumbered in the region hidden under the mask. Thus, although etching is much faster in the mask-edge region, it is not as fast as the straightforward perturbation analysis of Section 3.1.1 predicts.

We remark in passing that the parameter σ no longer appears in the explicit part of Equation (64). This is a pleasing observation, since that parameter arose in [4] in a part of that analysis which has no bearing on the problem discussed in the present paper.

[1] A personal communication with the authors of [11] clarified two misprints in their paper: on p. 173, line 4, the power −2/3 should read −7/3; the power 1/3 in the third displayed equation on p. 173 should read −1/3.

3.2. Deep cavities ($\tau \gg \beta$)

We shall now turn to the etching of deep cavities, *i.e.*, $\eta_0(\theta, \tau) \gg 1$. Because of the inertness of both boundaries $\theta = 0$ and $\theta = \frac{1}{2}\pi$, since $\partial C/\partial\theta = 0$, it can be understood, on physical grounds, that η_0 will become independent of θ eventually, that is, for sufficiently large τ. The appropriate τ-regime far exceeds the right-most bound of Equation (38). Thus, invoking the quasi-stationary model, we have Equation (32), but now with

$$C = 1 \quad \text{at} \quad \eta = -\eta_0 \,. \tag{65}$$

Again, we find a solution independent of θ that reads:

$$C = \frac{\frac{1}{2}\pi - \arctan \mathrm{e}^{\eta}}{\frac{1}{2}\pi - \arctan \mathrm{e}^{-\eta_0}} \,. \tag{66}$$

Inserting this into the equation for the moving boundary (26), we have

$$\frac{\mathrm{d}\eta_0}{\mathrm{d}\tau} \sim \frac{1}{\pi\beta}\frac{1}{\cosh^3 \eta_0} \,, \tag{67}$$

where the term arctan $\mathrm{e}^{-\eta_0}$ has been set equal to zero in view of the limit $\eta_0 \to \infty$. Also, since $\cosh \eta_0 \gg 1$, the term $\cos^2\theta$ can be disregarded in this leading-order analysis. In fact, this observation is in line with our assumption that eventually the solution will be independent of θ. This being an asymptotic analysis describing the final stages of the etching process for $\tau \to \infty$, it is impossible to impose an initial condition. Therefore, the general solution involves a time-shift parameter τ_0. Integrating (67), retaining the dominant term only, that is, using the approximation

$$\cosh \eta_0 \sim \tfrac{1}{2}\mathrm{e}^{\eta_0} \,, \tag{68}$$

we have

$$\eta_0 \sim \frac{1}{3}\log\left(\frac{24}{\pi\beta}(\tau + \tau_0)\right) . \tag{69}$$

It is obvious that this solution applies only when $\tau \gg \beta$; this time regime is completely outside the range defined by Equation (38), as it should be.

Recasting Equation (69) in terms of the original Cartesian coordinates through (9–11), dropping the time-shift parameter τ_0 and using dimensional variables, we have

$$z_b \sim -\left(\tfrac{3}{\pi}c_0\sigma_{\mathrm{e}}at\right)^{\frac{1}{3}} \,, \tag{70}$$

which shows that eventually the depth of etching z_b progresses as the one-third power of the time when $z_b \gg a$. The etched cavity approaches a spherical shape. The actual time regime in which this occurs is

$$t \gg \frac{a^2}{c_0\sigma_{\mathrm{e}}} = \beta\frac{a^2}{D} \,. \tag{71}$$

It is interesting to note from (70) that the total volume etched out is

$$V = \frac{2}{3}\pi|z_b|^3 = 2c_0\sigma_{\mathrm{e}}at \,, \tag{72}$$

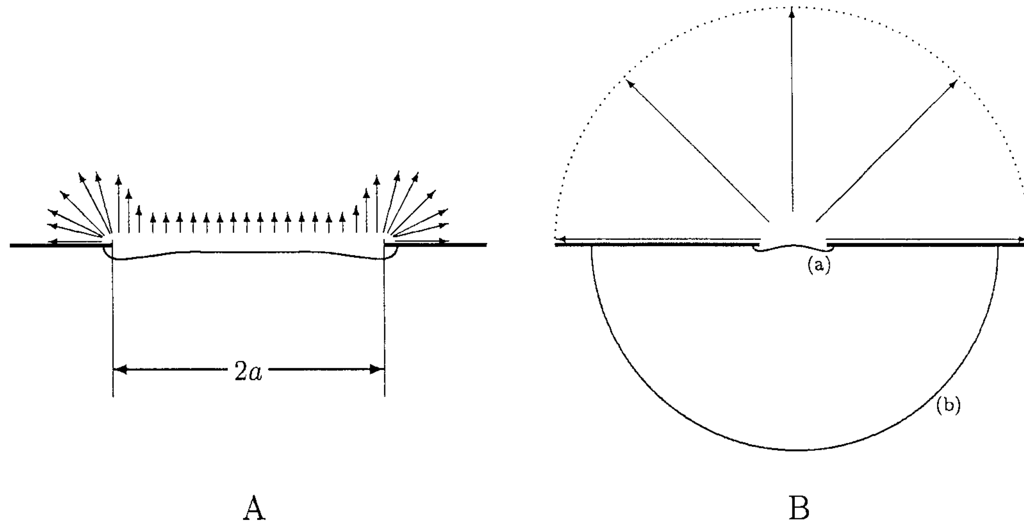

Figure 5. Schematic illustration of the various time regimes. Part A depicts the initial stage when the diffusion field, as indicated by the upper arrows, has not yet progressed far into the etchant; here the arrows indicate symbolically the strength of the concentration gradients. In B the diffusion field has become stationary; here the arrows and the dotted circle indicate symbolically the uniform spatial extent of the diffusion field. Further, (a) refers to the case described in Section 3.1 and (b) to that in Section 3.2.

which is proportional to t. This corresponds to the fact that the diffusion field outside the cavity assumes a steady state, which corresponds to a constant source strength. One could consider this as the result of an outer diffusion field that is fed continually by the value (for $\eta_0 \gg 1$)

$$C = \frac{\pi/4}{\frac{\pi}{2} - \arctan \mathrm{e}^{-\eta_0}} \sim \frac{1}{2} \tag{73}$$

at $\eta = 0$, which is in the mask opening in the plane of the mask. This result follows by substitution of $\eta = 0$ in Equation (66). Thus, for deep holes, the concentration in the mask opening is very close to half of that of the pure etchant, which means that, eventually, the concentration drop outside the cavity is the same as that within the cavity.

4. Results and discussion

The various time regimes, and their positions within the general time frame, are illustrated schematically in Figure 5. In Figure 5A the situation of the initial time regime has been sketched. The arrows above the plane of the substrate are indicative of the strength of the diffusion field c, with long arrows meaning large gradients. The spatial extent of this field above the plane is much less than $2a$, which is the diameter of the aperture. This time regime prevails as long as

$$t \ll \frac{a^2}{D}. \tag{74}$$

For small apertures ($a < 10^{-5}$m) this is less than a second and therefore of limited importance for a typical etching process lasting at least several minutes. In this time regime

diffusion is essentially a one-dimensional process in the central part of the aperture, but fully two-dimensional in the mask-edge region. This problem was considered in [4]. The analysis revealed a strong mask-edge effect.

The time regimes considered in this paper are sketched in Figure 5B. They occur for

$$t \gg \frac{a^2}{D}, \tag{75}$$

when the diffusion field, as indicated by the arrows, is fully developed and stationary. For these larger times we succeeded in finding two distinct time regimes for which the problem was amenable to asymptotic analysis. The first of these regimes, indicated by (a), is defined by (38). It is valid as long as the depth of etching is small in comparison with the width of the aperture. The second time regime refers to $\tau \gg \beta$, when the depth of etching far exceeds the width of the mask opening.

The advantage of the asymptotic solutions is, of course, that these afford a means of determining explicitly how the etching process depends upon the various physical parameters; they also lend structure to the problem as a whole in that they accentuate its salient features. A fully numerical approach is needed to determine the temporal development of the etching surface outside these specific time regimes. It cannot be denied, however, that the structure alluded to above should be of great help in carrying out the numerical task and interpreting the results derived therefrom.

We shall now interpret our results to see how the etched depth depends upon the physical parameters. From (24), (29), (39) and (62) we have the following expression for the depth in the centre ($\theta = \frac{1}{2}\pi$) of the etched pit for case (a) as depicted in Figure 5B, that is, for shallow pits:

$$|z_b| \approx \frac{2}{\pi}\frac{\sigma_e c_0 t}{a} = \frac{2}{\pi}\frac{Dt}{a}\frac{c_0 M_s}{m\rho_s}, \tag{76}$$

where we have used [5, Equation 9] to derive the right-most part of (76). Here M_s is the molecular weight of the solid (kg/kmol), ρ_s its density (kg/m^3) and m the number of molecules of active etching component required to dissolve one molecule of the solid. Clearly, in (76) the right-most fraction is a dimensionless group and the one preceding it has the dimension of length. Thus, for $1 \ll \tau \ll \beta$, the etched depth is inversely proportional to a. In other words: smaller holes etch raster (compare $\mathrm{d}|z_b|/\mathrm{d}t$) than bigger ones. Of course, one should keep in mind that, for this law to hold, there must only be diffusional transport and the diffusion field must be fully developed ($\tau \gg 1$). At short distances, diffusion is a very powerful transport mechanism. When the source gets smaller, the diffusion gradient near the source becomes larger, namely $\mathcal{O}(c/a)$, hence the increased etch rate.

The underetch effect follows a rule different from that shown in (76). From (62), (64), (24), (29) and the definition of σ_e given in [5], we have

$$r|_{\theta=0} - a = a\,\cosh\,\eta_0 - a \sim \frac{1}{2}a\eta_0^2 = \frac{3}{2(2\pi)^{2/3}}\left(\frac{D^2t^2}{a}\right)^{1/3}\left(\frac{c_0 M_s}{m\rho_s}\right)^{2/3} \tag{77}$$

for the distance etched under the mask. The maximum depth of etching occurs in the immediate vicinity of the mask, as was shown before in [4]. It follows the same rule as that of Equation (77), but the coefficient is twice that of (77). This follows from [11] and the footnote below the present Equation (63). Again, the depth of etching increases as a gets smaller, but the effect is less pronounced than that of (76) which applies to the centre of the cavity.

The corresponding result for case (b) of Figure 5B, which applies to deep holes, that is for $\tau \gg \beta$, follows from Equation (70) and [5, Equation 8], namely

$$|z_b| \approx (\frac{2}{\pi})^{1/3}(Dta)^{1/3}\left(\frac{c_0 M_s}{m\rho_s}\right)^{1/3}. \tag{78}$$

It follows that smaller holes now etch more slowly than bigger ones, where again the above provisos should be heeded. Reference [9, p. 64] shows results of the deep etching of four cavities with mask-opening sizes of 4, 10, 50 and 100 μm. In these experiments silicon wafers were etched with an hydrogen-fluoride (HF) solution. The etching times were the same for each result and of the order of an hour. The corresponding depths of etching were 49, 56, 68 and 77 μm, showing indeed a trend similar to that of Equation (78). A direct comparison is impossible for the following reasons: (i) in [9] etching occurred through slits instead of round apertures; (ii) there is no way of knowing that convection effects were suppressed sufficiently. Convection may have played a role, particularly for the larger mask-opening sizes, since HF etching of silicon generates heat. Even so, the comparison is satisfactory in that the trend is fully corroborated. The explanation given by Tjerkstra [9, p. 65] for the slower etching of smaller, deep holes appears to be the correct one. All of the etched material must perforce leave the cavity through a narrow aperture before it can diffuse freely into the etchant outside. Apparently, this effect tends to become stronger, the smaller the mask opening. Further experimental results on two-dimensional wet-chemical diffusion-controlled etching can be found in [2, Figures 8.10 and 8.11].

Apart from the opposite trend of $|z_b|$ with respect to a, as expressed by Equations (76) and (77) on the one hand and Equation (78) on the other, its behaviour *vis-à-vis* c_0, D and t is the same for the two cases, albeit that the exponent is different. In full agreement with what can be expected intuitively, $|z_b|$ increases when any of these parameters increases. It is interesting to note that the exponents of t, D and c_0 are equal to unity in (76), have the lower value of $\frac{2}{3}$ in (74) and reach a minimum value of $\frac{1}{3}$ in (78).

5. Concluding remarks

In this paper we have presented solutions describing the temporal development of an etching surface for wet-chemical diffusion-controlled etching of a substrate that is covered by an impenetrable mask featuring a round aperture. By applying asymptotic techniques, we succeeded in finding solutions pertaining to two separate time regimes. The analysis has been greatly facilitated by the observation that, in three-dimensional space, a diffusion field resulting from a finite-size source eventually becomes stationary. For small cavities this stationary state is attained within a time span that is only a small fraction of the total etching time. Because of this, the analysis of the three-dimensional problem is simpler than that of the corresponding one in two dimensions [7].

Two different time regimes were recognized as being particularly amenable to asymptotic analysis leading to explicit results. The first of these occurs when the etched cavity is still shallow. This case reveals the now well-known phenomenon of fast etching near mask edges in the diffusion-controlled etching regime. It was found that small holes etch faster than ones that are wider. In the second time regime, when etching has gone down to depths much greater than the width of the mask aperture, the opposite effect is shown: the etching speed decreases as the aperture gets smaller.

There is ample room for further research regarding this particular problem. An attempt could be made to raise the asymptotics to higher levels of accuracy by adding further terms. This, while being possibly interesting from a mathematical point of view, would not substantially increase our knowledge of the physics of the problem as laid down, for instance, in the Equations (76–78). Having understood the basic physics underlying this problem, as we have attempted to do in this paper, one should now proceed to solve the basic system of governing equations numerically, so as to get a full overview of the temporal development of the etching surface. Work is in progress to achieve this [13].

Finally, we remark that it is absolutely essential that models of a kind as investigated here be validated by suitable experimentation. Partial, be it qualitative, support for some of our results has already been furnished by [9]. Careful experiments are needed to be able to bring theory and experiment on an equal footing, so as to serve as ideal complements of one another. Only then will it be possible to combine theory and experiment to determine accurate values of the physical parameters, supposing, of course, that these experiments confirm the theory.

Acknowledgement

The author gratefully acknowledges financial support by the Dutch Technology Foundation (STW). This research is part of STW project TWI.5453 entitled 'Analysis and Control of Transport Phenomena in Wet-Chemical Etching Processes'. The criticism of the referees has resulted in the removal of a number of inaccuracies of expression from an earlier draft.

References

1. D.M. Allen, *The Principles and Practice of Photochemical Machining and Photoetching*. Bristol: Hilger (1986) 190pp.
2. P.H.L. Notten, J.A.E.M. van den Meerakker and J.J. Kelly, *Etching of III-IV Semiconductors*. Oxford: Elsevier Adv. Techn. (1991) 349pp.
3. M.C. Elwenspoek and H. Jansen, *Silicon Micromachining*. Cambridge: CUP (1998) 405pp.
4. H.K. Kuiken, Etching: a two-dimensional mathematical approach. *Proc. R. Soc. London* A392 (1984) 199–225.
5. H.K. Kuiken, J.J. Kelly and P.H.L. Notten, Etching profiles at resist edges. I. Mathematical models for diffusion-controlled cases. *J. Electrochem. Soc*. 133 (1986) 1217–1226.
6. P.H.L. Notten, J.J. Kelly and H.K. Kuiken, Etching profiles at resist edges. II. Experimental confirmation of models using GaAs. *J. Electrochem. Soc*. 133 (1986) 1226–1232.
7. H.K. Kuiken, Etching through a slit. *Proc. R. Soc. London* A396 (1984) 95–117.
8. C. Vuik and C. Cuvelier, Numerical solution of an etching problem. *J. Comp. Phys*. 59 (1985) 247–263.
9. R.W. Tjerkstra, *Isotropic Etching of Silicon in Fluoride Solutions as a Tool for Micromachining*. Doctoral Thesis, University of Twente, The Netherlands (1999) 132 pp.
10. P. Moon and D.E. Spencer, *Field Theory Handbook*, third corrected printing. Berlin: Springer (1988) 236pp.
11. S.D. Howison and J.R. King, Explicit solutions to six free-boundary problems in fluid flow and diffusion. *IMA J. Appl. Math*. 42 (1989) 155–175.
12. P. Ya. Polubarinova-Kochina, *Theory of Groundwater Movement*. Princeton: Princeton U. Press (1962) 613pp.
13. J.J. Sudirham, *Forthcoming PhD Thesis*, U. Twente, Enschede, The Netherlands.